SUSY QCD Corrections to Associated Higgs-bottom Quark Production

S. Dawson and C. B. Jackson

Department of Physics, Brookhaven National Laboratory, Upton, NY 11973, USA

Abstract

The associated production of a Higgs boson with a b quark is a discovery mode for an MSSM Higgs boson at large $\tan\beta$. We compute the SUSY QCD corrections from gluino and squark loops to this process and combine them with the $\mathcal{O}(\alpha_s^2)$ NLO QCD corrections to obtain reliable predictions for the rate. Finally, we compare our results with an effective Lagrangian approximation which includes only the low energy corrections from squark and gluino loops to the $b\bar{b}$ Higgs vertices.

I. INTRODUCTION

The search for the Higgs boson is among the most important challenges facing the current generation of colliders. If there is a single Higgs boson with the properties predicted by the Standard Model, we expect that it will be discovered at either the Tevatron or the LHC, with the optimal channel for discovery depending strongly on the Higgs mass. In the Standard Model, the production of a Higgs boson in association with b quarks is never important. However, in the minimal supersymmetric model (MSSM), there are five Higgs bosons–two neutral Higgs bosons, h^0 and H^0, a pseudoscalar, A^0, and two charged Higgs bosons, $H^{\pm}$– and the strategy for discovery is quite different from in the Standard Model. In the MSSM, the couplings of the Higgs bosons to b quarks can be significantly enhanced and for a large range of parameter space, Higgs production in association with b quarks is the most likely discovery channel[1, 2, 3, 4, 5].

The production of a Higgs boson in association with a b quark has been extensively studied[1, 2, 3, 4, 5, 6, 7, 8, 9, 10, 11] and the NLO QCD corrections are well understood, both in the 4- and 5- flavor number parton schemes[1, 3, 8]. In the 4- flavor number scheme, the lowest order processes for producing a Higgs boson and a b quark are $gg \to b\bar{b}\phi$ and $q\bar{q} \to b\bar{b}\phi$[4, 6, 10]. (The neutral Higgs bosons are generically, $\phi = h^0, H^0, A^0$). In a 5- flavor number scheme, the b quark appears as a parton and potentially large logarithms of the form $\ln(\frac{M_\phi}{m_b})$ are absorbed into b quark parton distribution functions (PDFs)[12, 13]. In the 5- flavor number scheme, the lowest order process for producing a Higgs boson in association with b quarks is $b\bar{b} \to \phi$ when no b quarks are tagged in the final state and $bg \to b\phi$ when a single b quark is tagged[1, 3, 4, 6, 10]. Contributions from the gg and $q\bar{q}$ initial states are thus subleading in the $5-$ flavor number scheme. Although the 4- and 5- flavor number schemes represent different orderings of perturbation theory, the two schemes have been shown to yield equivalent numerical results. The residual renormalization and factorization scale, scheme, and PDF uncertainties of the NLO calculations result in a $10-20\%$ uncertainty on the prediction of the rate[1, 3].

When no b quarks are tagged in the final state, the dominant production mechanism in the 5-flavor number scheme is $b\bar{b} \to \phi$, which has been calculated to NNLO[14]. When a single b quark is tagged, the rate is lower, but so also is the background and it is this channel which we focus on here. Both CDF and D0 have derived limits on $\tan\beta$ from

2

Tevatron data, based on the search for $p\overline{p} \to b\phi$ with $\phi \to \tau^+\tau^-$ and $\phi \to b\overline{b}$[15]. In this paper, we present the $\mathcal{O}(\alpha_s^2)$ SUSY QCD (SQCD) corrections from gluino-squark loops to the b- Higgs production processes. Gluino-squark virtual contributions have been shown to be significant for the inclusive $b\overline{b} \to \phi$ channel[16] and it is of interest to examine the SQCD corrections for the case where a single b quark is tagged along with the Higgs boson.[1] These corrections, along with the NLO QCD corrections previously computed,[4, 6, 11] and the summation of the logarithmic threshold corrections[21], can then be used to obtain reliable $\mathcal{O}(\alpha_s^2)$ predictions.

An effective Lagrangian approach has been extensively used in the literature to include SQCD effects to the $b\overline{b}\phi$ vertex[22, 23, 24] since these corrections are enhanced for large values of $\tan\beta$. The effective Lagrangian is derived assuming $M_\phi << M_{SUSY}$, where M_{SUSY} is a typical squark or gluino mass scale. We investigate the range of validity of the effective Lagrangian approach for computing the SQCD corrections to the $b\phi$ production process. In addition, we consider the decoupling properties of our results for heavy MSSM mass scales. For the decay process, $h^0 \to b\overline{b}$, heavy SUSY particles do not decouple unless the pseudoscalar mass, M_A, is also large with respect to the electroweak scale[25, 26] and we observe a similar phenomena in our results.

In Section 2, we discuss the general MSSM framework of our calculation and the effective Lagrangian approach for approximating the SQCD contributions of squarks and gluinos. Section 3 contains the lowest order results for the production process, $bg \to b\phi$, a discussion of the renormalization framework for the SQCD NLO contributions, and the SQCD NLO results. Numerical results for the Tevatron and the LHC, along with a discussion of the decoupling properties of the SQCD contributions are given in Section 4 and analytic results for the SQCD corrections are gathered in an appendix. Finally, in Section 5, we present some conclusions. Section 5 contains predictions for the $b\phi$ cross sections at the Tevatron and the LHC which contain all known $\mathcal{O}(\alpha_s^2)$ contributions and thus are the most reliable calculations available.

---

[1] Correction to Higgs plus jet production in the MSSM from the gg initial state have been examined in Refs. [17, 18, 19, 20].

II. FRAMEWORK

A. MSSM Basics

The MSSM has been extensively studied in the literature and comprehensive reviews can be found in Refs. [27, 28]. Here we briefly summarize those aspects of the MSSM relevant for our calculation.

In the MSSM, there are two $SU(2)_L$ Higgs doublets, H_u and H_d, which can be written as[27, 28, 29],

$$H_d = \begin{pmatrix} h_d^+ \\ \frac{1}{\sqrt{2}}(v_1 + h_d^0 + i\chi_d^0) \end{pmatrix}, \quad H_u = \begin{pmatrix} \frac{1}{\sqrt{2}}(v_2 + h_u^0 - i\chi_u^0) \\ -h_u^- \end{pmatrix}. \tag{1}$$

After spontaneous symmetry breaking, the W and Z bosons obtain masses and fix $v_{SM}^2 = v_1^2 + v_2^2 = (246 \text{ GeV})^2$, while the ratio of the VEVs, $\tan\beta = \frac{v_2}{v_1}$, is a free parameter of the theory. There are five physical Higgs bosons, h^0, H^0, A^0 and $H^\pm$, remaining in the theory.

The scalar potential of the MSSM is described at tree level by two free parameters, which are usually taken to be $\tan\beta$ and the mass of the pseudoscalar Higgs boson, M_A. In terms of these parameters, the remaining scalar masses, $M_{H^\pm}, M_h$ and M_H, are predicted quantities with,

$$M_{H^\pm}^2 = M_A^2 + M_W^2. \tag{2}$$

The physical neutral Higgs bosons, h^0 and H^0, are linear combinations of h_d^0 and h_u^0,

$$\begin{pmatrix} h^0 \\ H^0 \end{pmatrix} = \begin{pmatrix} c_\alpha & -s_\alpha \\ s_\alpha & c_\alpha \end{pmatrix} \begin{pmatrix} h_u^0 \\ h_d^0 \end{pmatrix} \tag{3}$$

where $c_\alpha \equiv \cos\alpha$ and $s_\alpha \equiv \sin\alpha$. The neutral Higgs boson masses at tree level are given by,

$$M_{h,H}^2 = \frac{1}{2}\left\{ M_A^2 + M_Z^2 \mp \sqrt{(M_A^2 + M_Z^2)^2 - 4M_Z^2 M_A^2 \cos^2 2\beta} \right\}. \tag{4}$$

Eq. 4 implies a tree level upper bound on the lightest Higgs boson mass, $M_h(tree) < M_Z$. Furthermore, at tree-level,

$$\tan 2\alpha = \tan 2\beta \left(\frac{M_A^2 + M_Z^2}{M_A^2 - M_Z^2} \right). \tag{5}$$

4

The predictions of Eqs. 4 and 5 receive large radiative corrections of $\mathcal{O}(G_F m_t^4)$ which raise the lower bound on m_h to $130 - 140$ GeV.[2] We include these corrections using the program FeynHiggs, which generates an effective mixing angle, α_{eff}, and radiatively corrected values for the Higgs boson masses[30]. Using α_{eff} in the tree level couplings incorporates the bulk of the MSSM corrections to the Higgs masses and mixing angles[31].

The MSSM Yukawa couplings are given at tree level by,

$$L_{YUK} = -\lambda_b \overline{\psi}_L H_d b_R - \lambda_t \overline{\psi}_L H_u t_R + h.c. , \tag{6}$$

where $\psi_L^\dagger = (t_L, b_L)$. Eq. 6 generates masses for the t and b quarks,

$$\begin{aligned} m_b &= \frac{\lambda_b v_1}{\sqrt{2}} \\ m_t &= \frac{\lambda_t v_2}{\sqrt{2}} . \end{aligned} \tag{7}$$

We note that the bottom quark only couples to H_d, while the top quark only couples to H_u. In terms of the physical Higgs mass eigenstates,

$$\begin{aligned} L_{YUK} &= -\frac{m_b}{v_{SM}} \left(-\frac{s_\alpha}{c_\beta} \overline{b} b h^0 + \frac{c_\alpha}{c_\beta} \overline{b} b H^0 - t_\beta \overline{b} i \gamma_5 b A^0 \right) \\ &\equiv \Sigma g_{\overline{b} b \phi_i}^{LO} \overline{b} b \phi_i , \end{aligned} \tag{8}$$

where $c_\beta = \cos\beta$, $s_\beta = \sin\beta$, and $t_\beta = \tan\beta$. We see that the Yukawa couplings to the b quark are enhanced for large values of $\tan\beta$.

In the MSSM, the scalar partners of the left- and right- handed b quarks, $\tilde{b}_L$ and $\tilde{b}_R$, are not mass eigenstates, but mix according to,

$$L_M = -(\tilde{b}_L^*, \tilde{b}_R^*) M_{\tilde{b}}^2 \begin{pmatrix} \tilde{b}_L \\ \tilde{b}_R \end{pmatrix} . \tag{9}$$

The $\tilde{b}$ squark mass matrix is,

$$M_{\tilde{b}}^2 = \begin{pmatrix} \tilde{m}_L^2 & m_b(A_b - \mu \tan\beta) \\ m_b(A_b - \mu \tan\beta) & \tilde{m}_R^2 \end{pmatrix} , \tag{10}$$

---

[2] The upper bound on the lightest Higgs mass depends on the stop mass, as well as other MSSM parameters. For a review see Ref. [28].

where we define,

$$\tilde{m}_L^2 = M_Q^2 + m_b^2 + M_Z^2 \cos 2\beta (I_3^b - Q_b \sin^2 \theta_W)$$

$$\tilde{m}_R^2 = M_D^2 + m_b^2 + M_Z^2 \cos 2\beta Q_b \sin^2 \theta_W \,, \tag{11}$$

and $M_{Q,D}$ are the soft SUSY breaking masses, $I_3^b = -1/2$, and $Q_b = -1/3$. The parameter A_b is the trilinear scalar coupling of the soft supersymmetry breaking Lagrangian and μ is the Higgsino mass parameter. The b squark mass eigenstates are $\tilde{b}_1$ and $\tilde{b}_2$ and define the b-squark mixing angle, $\tilde{\theta}_b$

$$\tilde{b}_1 = \cos \tilde{\theta}_b \tilde{b}_L + \sin \tilde{\theta}_b \tilde{b}_R$$

$$\tilde{b}_2 = -\sin \tilde{\theta}_b \tilde{b}_L + \cos \tilde{\theta}_b \tilde{b}_R \,, \tag{12}$$

where at tree level,

$$\tan 2\tilde{\theta}_b = \frac{m_b(A_b - \mu \tan \beta)}{\tilde{m}_L^2 - \tilde{m}_R^2} \,. \tag{13}$$

Eq. 10 gives the squark mass eigenstates at tree level,

$$m_{\tilde{b}_{1,2}}^2 = \left(\tilde{m}_L^2 \cos^2 \tilde{\theta}_b + \tilde{m}_R^2 \sin^2 \tilde{\theta}_b \right) \mp \sin(2\tilde{\theta}_b) m_b (A_b - \mu \tan \beta) \,. \tag{14}$$

The b squarks (unlike the b quark) couple to both Higgs doublets, H_u and H_d and the Feynman rules for the squark-squark-Higgs couplings can be found in the appendices of Ref. [27]. Finally, we use the Feynman diagramatic techniques of Ref [32] and the Feynman rules for the squark/gluino interactions which are given in Appendix A of Ref. [33].

B. Effective Lagrangian Approach

At tree level, there is no $\overline{\psi}_L b_R H_u$ coupling in the MSSM (see Eq. 6), but such a coupling arises at one loop through the Feynman diagram shown in Fig. 1 and gives rise to an effective interaction[22, 23],

$$L_{eff} = -\lambda_b \overline{\psi}_L \left(H_d + \frac{\Delta m_b}{\tan \beta} H_u \right) b_R + h.c. \quad . \tag{15}$$

Eq. 15 shifts the b quark mass from its tree level value,

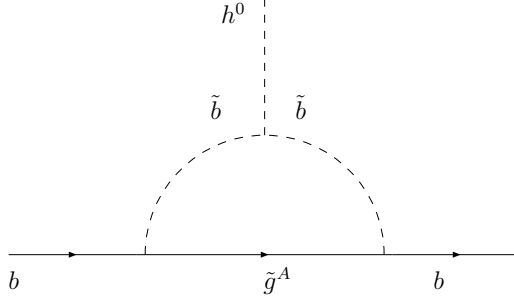$$m_b = \frac{\lambda_b v_1}{\sqrt{2}} (1 + \Delta m_b) \,, \tag{16}$$

6

FIG. 1: SUSY QCD contribution from gluinos and squarks to the $b\bar{b}h^0$ effective vertex. Both squarks, $\tilde{b}_1$ and $\tilde{b}_2$, contribute to the interaction.

and also implies that the Yukawa couplings of the Higgs bosons to the b quark are shifted from the tree level predictions. The shift of the Yukawa couplings can be included with an effective Lagrangian approach[22, 26],

$$
\begin{aligned}
L_{eff} &= -\frac{m_b}{v_{SM}}\left(\frac{1}{1+\Delta m_b}\right)\left(-\frac{\sin\alpha}{\cos\beta}\right)\left(1-\frac{\Delta m_b}{\tan\beta\tan\alpha}\right)\bar{b}bh^0 \\
&\quad -\frac{m_b}{v_{SM}}\left(\frac{1}{1+\Delta m_b}\right)\left(\frac{\cos\alpha}{\cos\beta}\right)\left(1+\frac{\Delta m_b\tan\alpha}{\tan\beta}\right)\bar{b}bH^0 \\
&\quad -\frac{m_b}{v_{SM}}\left(\frac{1}{1+\Delta m_b}\right)\left(-\tan\beta\right)\left(1-\frac{\Delta m_b}{\tan^2\beta}\right)\bar{b}i\gamma_5 bA^0 \\
&\equiv g_{b\bar{b}h}\bar{b}bh^0 + g_{b\bar{b}H}\bar{b}bH^0 + g_{b\bar{b}A}\bar{b}i\gamma_5 bA^0 \, .
\end{aligned}
\tag{17}
$$

The Lagrangian of Eq. 17 has been shown to sum all terms of $\mathcal{O}(\alpha_s^n\tan^n\beta)$ for large $\tan\beta$[22].[3] This effective Lagrangian has been used to compute both the inclusive production process, $b\bar{b}\to h^0$, and the decay process, $h^0\to b\bar{b}$, and yields results which are within a few percent of the exact one-loop SQCD calculations[16, 26].

The expression for Δm_b is found in the limit $m_b << m_\phi, M_Z << m_{\tilde{b}_1}, m_{\tilde{b}_2}, m_{\tilde{g}}$. The contribution to Δm_b from sbottom/gluino loops is[22, 23, 34]

$$
\Delta m_b = \frac{2\alpha_s(\mu_R)}{3\pi}m_{\tilde{g}}\mu\tan\beta I(m_{\tilde{b}_1}, m_{\tilde{b}_2}, m_{\tilde{g}}) \, ,
\tag{18}
$$

where the function $I(a, b, c)$ is,

$$
I(a, b, c) = \frac{1}{(a^2-b^2)(b^2-c^2)(a^2-c^2)}\left\{a^2b^2\log\left(\frac{a^2}{b^2}\right) + b^2c^2\log\left(\frac{b^2}{c^2}\right) + c^2a^2\log\left(\frac{c^2}{a^2}\right)\right\} \, ,
\tag{19}
$$

---

[3] It is also possible to sum the contributions which are proportional to A_b, but these terms are less important numerically[26].

FIG. 2: Feynman diagrams for $g(q_1) + b(q_2) \to b(p_b) + \phi_i(p_h)$, where $\phi_i = h^0, H^0$ or A^0.

and $\alpha_s(\mu_R)$ should be evaluated at a typical squark or gluino mass. Note that Eq. 18 is valid for arbitrary values of $\tan\beta$. There is also an electroweak correction to Δm_b which we neglect, since we are concerned only with the $\mathcal{O}(\alpha_s^2)$ contributions in this paper.

Eq. 18 is a non-decoupling effect in the sense that if the mass scales of the squarks and gluino, along with the mixing parameter μ, become large for fixed M_A, Δm_b does not vanish,

$$\Delta m_b \to -sign(\mu)\frac{\alpha_s}{3\pi}\left(\tan\beta + \cot\alpha\right). \tag{20}$$

In the large M_A limit,

$$\tan\beta + \cot\alpha \to -\frac{2M_Z^2}{M_A^2}\tan\beta\cos 2\beta + \mathcal{O}\left(\frac{M_Z^4}{M_A^4}\right), \tag{21}$$

and the decoupling limit of the MSSM is recovered[25].

In the next sections, we investigate the use of the effective Lagrangian of Eq. 17 to estimate the SQCD corrections to the process $gb \to b\phi$ and compare the results with the complete $\mathcal{O}(\alpha_s^2)$ one-loop SQCD calculation.

III. $gb \to b\phi$ AT NLO IN SUSY QCD

In this section, we summarize the expressions for the SQCD corrections to the $gb \to b\phi$ process.

A. Lowest Order

The tree level diagrams for $g(q_1) + b(q_2) \to b(p_b) + \phi(p_h)$ are shown in Fig. 2. The lowest order amplitude can be written as a linear sum over two allowed kinematic structures, with

a third contributing at NLO,[4]

$$M_s^\mu = \bar{u}(p_b)(\slashed{q}_1 + \slashed{q}_2)\gamma^\mu u(q_2)$$

$$M_t^\mu = \bar{u}(p_b)\gamma^\mu(\slashed{p}_b - \slashed{q}_1)u(q_2)$$

$$M_1^\mu = q_2^\mu \bar{u}(p_b)u(q_2)\,. \tag{22}$$

The Born level amplitude is

$$A_{Born}^\mu = g_s T^a g_{b\bar{b}\phi_i}^{LO} A_{LO}^\mu\,, \tag{23}$$

where,

$$A_{LO}^\mu = \left(\frac{M_s^\mu}{s} + \frac{M_t^\mu}{t}\right)\,, \tag{24}$$

and we define the usual Mandelstam variables as:

$$s \equiv (q_1 + q_2)^2 = (p_b + p_h)^2\,,$$

$$t \equiv (q_1 - p_b)^2 = (q_2 - p_h)^2\,,$$

$$u \equiv (q_1 - p_h)^2 = (q_2 - p_b)^2\,. \tag{25}$$

The spin and color averaged tree level partonic cross section is,

$$\frac{d\hat{\sigma}_{Born}}{dt}(bg \to b\phi) = \frac{\alpha_s(\mu_R)}{96s^2}\left(g_{b\bar{b}\phi}^{LO}\right)^2 \mid A_{LO}^\mu \mid^2\,. \tag{26}$$

The lowest order, $\mathcal{O}(\alpha_s)$, hadronic cross section is found in the usual manner by integration with the b quark and gluon PDFs,

$$\sigma_{LO}(pp \to b\phi) = \int dx_1 dx_2 \left[g(x_1, \mu_F)b(x_2, \mu_F)\int dt\left(\frac{d\hat{\sigma}_{Born}}{dt}\right) + (x_1 \leftrightarrow x_2)\right]\,. \tag{27}$$

B. NLO QCD Corrections

The NLO pure QCD $\mathcal{O}(\alpha_s^2)$ corrections to the $gb \to b\phi$ process consist of one-loop virtual corrections containing b quarks and gluons and real gluon emission diagrams, along with appropriate counterterms. These corrections have been computed by several groups with excellent agreement between the groups[1, 3, 4, 6, 7, 8, 10, 11]. Schematically,

$$\sigma_{NLO}(pp \to b\phi)_{QCD} \equiv \left(\frac{g_{b\bar{b}\phi}}{g_{b\bar{b}\phi}^{LO}}\right)^2 \sigma_{LO}(pp \to b\phi) + \delta\sigma_{QCD}(pp \to b\phi)$$

$$\equiv \sigma_{NLO}(\text{gluon only})\,. \tag{28}$$

---

[4] For pseudoscalar production, the three kinematic structures of Eq. 22 include a γ_5.

In Eq. 28, we normalize the Yukawa couplings for both the Born contribution to the NLO cross section and for $\delta\sigma_{QCD}$ with $g_{b\bar{b}\phi}$ (defined by the effective Lagrangian of Eq. 17). This algorithm for including the Yukawa couplings of Eq. 17 in the NLO QCD corrections corresponds to the convention of Ref. [1] and so the NLO QCD corrections presented in Section 4 (and labelled "NLO (gluon only)") can be directly compared with this reference.

C. Improved Born Approximation

One of the major goals of this work is to investigate the accuracy of the Improved Born Approximation (IBA). In order to make the comparison as transparent as possible, we define an Improved Born Approximation in which the Born amplitude is normalized by the Yukawa couplings, $g_{b\bar{b}\phi}$, of Eq. 17,

$$\frac{d\hat{\sigma}_{IBA}}{dt} \equiv \frac{d\hat{\sigma}_{Born}}{dt}\left(\frac{g_{b\bar{b}\phi}}{g_{b\bar{b}\phi}^{LO}}\right)^2.\tag{29}$$

The Improved Born Approximation incorporates the effective Lagrangian approximation to the SQCD effects on the $b\bar{b}\phi$ Yukawa couplings at low energy, but does not include the full SQCD calculation presented in the next section. In particular, the "Improved Born Approximation" does not include contributions from box diagrams including internal squarks and gluinos or the full momentum dependence of the SQCD contributions.

D. One Loop SQCD Corrections

The amplitudes for the SQCD one-loop corrections from sbottom/gluino loops can be written as:

$$\mathcal{A}_i^\mu = \frac{\alpha_s}{4\pi}(g_s T^a)\left[X_i^{(s)}M_s^\mu + X_i^{(t)}M_t^\mu + X_i^{(1)}M_1^\mu\right],\tag{30}$$

where the matrix elements M_s, M_t and M_1 are given in Eq. 22 and expressions for the individual contributions, X_i are found in Appendix B. The integrals of Appendix A are evaluated in $n = 4 - 2\epsilon$ dimensions. The diagrams consist of self-energy, vertex, and box contributions, along with the appropriate counterterms to cancel the ultraviolet divergences. We consistently neglect contributions which are suppressed by terms of $\mathcal{O}(m_b^2/s, m_b^2/M_\phi^2)$,

etc. The spin and color averaged partonic cross section to NLO in SQCD is,

$$
\frac{d\hat{\sigma}}{dt}(bg \to b\phi)_{SQCD} = \frac{d\hat{\sigma}}{dt}(bg \to b\phi)\,|_{IBA} + \frac{\alpha_s^2(\mu_R)}{192\pi s^2}\left(g_{b\bar{b}\phi}\right)^2 \sum_i |A_{LO} \cdot \left(X_i^{(s)} M_s^* + \right.
$$

$$
\left. X_i^{(t)} M_t^* + X_i^{(1)} M_1^* \right) + \frac{d\hat{\sigma}_{CT}}{dt}, \tag{31}
$$

where the contribution from the counterterms is discussed in the next section. The SQCD NLO contribution to the hadronic cross section is

$$
\sigma_{NLO}(pp \to b\phi)_{SQCD} = \int dx_1 dx_2 \left[g(x_1, \mu) b(x_2, \mu) \int dt \left(\frac{d\hat{\sigma}_{SQCD}}{dt} \right) + (x_1 \leftrightarrow x_2) \right]. \tag{32}
$$

The result of Eq. 32 is labelled "NLO (gluino/squark only)" in the figures of Section IV.

Finally, we note that

$$
|A_{LO} \cdot M_s^*| = -4 \left[\frac{tm_\phi^2 + u^2 + us}{t} \right]
$$

$$
|A_{LO} \cdot M_t^*| = -4 \left[\frac{sm_\phi^2 - us + um_\phi^2}{s} \right]
$$

$$
|A_{LO} \cdot M_1^*| = -2 \left[\frac{u^2 + us}{t} \right]. \tag{33}
$$

E.   Counterterms

In this section, we discuss the squark and gluino contributions to the counterterms which are necessary for the SQCD one-loop calculation. The renormalization of the pure QCD contribution has been presented previously[1, 3, 4, 6, 7, 8, 10, 11].

Self-energy and vertex corrections to the tree-level process $gb \to b\phi$ process give rise to ultraviolet (UV) divergences. These singularities are cancelled by a set of counterterms fixed by well-defined renormalization conditions. The renormalization of the propagators and interaction vertices of the theory reduces to introducing counterterms for the external field wavefunctions of the bottom quarks (δZ_V) and gluons (δZ_3), and for the strong coupling constant (δZ_g). The counterterm for the bottom quark Yukawa coupling, $g_{b\bar{b}\phi}^{LO} \sim m_b/v$, coincides with the counterterm for the bottom quark mass, since the vacuum expectation value v is not renormalized at the one-loop level of SUSY QCD. (We follow the approach of Refs. [33, 35] for the SQCD renormalization).
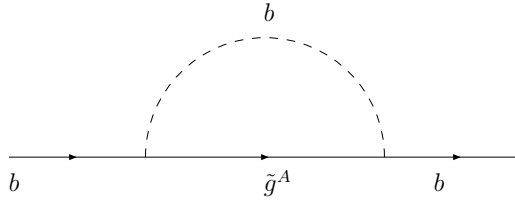
11

FIG. 3: SUSY QCD contribution to the b quark self energy. Both squarks, $\tilde{b}_1$ and $\tilde{b}_2$, contribute to the interaction.

We define the b quark self energy as

$$\Sigma^b(p) = \not{p}\left(\Sigma_V^b(p^2) - \Sigma_A^b(p^2)\gamma_5\right) + m_b\Sigma_S^b(p^2)$$

$$\delta\Sigma^b(p) = \not{p}\left(\delta Z_V^b - \delta Z_A^b\gamma_5\right) - m_b\delta Z_V^b - \delta m_b\,, \tag{34}$$

which yields the renormalized propagator, $\Sigma_{ren}^b(p) = \Sigma^b(p) + \delta\Sigma^b(p)$,

$$\Sigma_{ren}^b(p) = (\not{p} - m_b)\left(\Sigma_V^b + \delta Z_V^b\right) + m_b\left(\Sigma_V^b + \Sigma_S^b - \frac{\delta m_b}{m_b}\right)\,. \tag{35}$$

We evaluate the SQCD contribution to the b mass using the on-shell renormalization condition,

$$\Sigma^b(\not{p} = m_b) = 0$$

$$lim_{\not{p}\to m_b}\frac{\Sigma^b(p)}{\not{p} - m_b} = 0\,. \tag{36}$$

This scheme decouples the gluino and b-squark from the running of the b quark Yukawa coupling. The self energy contribution from gluino-squark loops is shown in Fig. 3 and yields the on-shell result,

$$\begin{aligned}
\frac{\delta m_b}{m_b} &= \left(\Sigma_V^b + \Sigma_S^b\right)|_{p^2=m_b^2} \\
&= -\frac{\alpha_s(\mu_R)}{3\pi}\Bigg\{B_1(m_b^2, m_{\tilde{g}}, m_{\tilde{b}_1}) + B_1(m_b^2, m_{\tilde{g}}, m_{\tilde{b}_2}) \\
&\quad +2\sin\tilde{\theta}_b\tilde{\cos}\theta_b\frac{m_{\tilde{g}}}{m_b}\left[B_0(m_b^2, m_{\tilde{g}}, m_{\tilde{b}_1}) - B_0(m_b^2, m_{\tilde{g}}, m_{\tilde{b}_2})\right]\Bigg\}\,,
\end{aligned} \tag{37}$$

where the integrals B_0 and B_1 are defined in Appendix A.

The b-quark self-energy is renormalized by $\Psi \to \sqrt{Z_V^b}\Psi = \sqrt{1 + \delta Z_V^b}\Psi$. Neglecting

contributions suppressed by powers of m_b, in the on-shell scheme we find,

$$
\begin{aligned}
\delta Z_V^b &= -\Sigma_V \big|_{p^2 = m_b^2} \\
&= \frac{\alpha_s(\mu_R)}{3\pi} \left\{ B_1(m_b^2, m_{\tilde{g}}, m_{\tilde{b}_1}) + B_1(m_b^2, m_{\tilde{g}}, m_{\tilde{b}_2}) \right\}.
\end{aligned}
\tag{38}
$$

The external gluon has the wavefunction renormalization, $g_\mu^A \to \sqrt{Z_3} g_\mu^A = \sqrt{1 + \delta Z_3} g_\mu^A$ and the renormalization of the strong coupling is found from $g_s \to Z_g g_s$. We have further, $\delta Z_g = -\delta Z_3/2$.[5] We renormalize g_s using the $\overline{MS}$ scheme modified to decouple heavy SUSY particles, *i.e.* the heavy squark and gluino contributions are evaluated at zero momentum[36],

$$
\begin{aligned}
\delta Z_3 &= -\frac{\partial \Sigma_T(p^2)}{\partial p^2} \big|_{pole} \\
&= -\frac{\alpha_s(\mu_R)}{4\pi} \left\{ \frac{1}{6} \Sigma_{\tilde{q}_i} \left(\frac{4\pi \mu_R^2}{m_{\tilde{q}_i}^2} \right)^\epsilon + 2 \left(\frac{4\pi \mu_R^2}{m_{\tilde{g}}^2} \right)^\epsilon \right\} \frac{1}{\epsilon} \Gamma(1 + \epsilon),
\end{aligned}
\tag{39}
$$

where Σ_T represents the transverse portion of the gluon self energy, the sum in Eq. 39 is over all squarks (not just the b squark), and μ_R is an appropriate renormalization scale.

The Yukawa couplings are defined by Eq.17, which includes the summation of large $\tan\beta$ effects. Using Eq. 17 for the Yukawa couplings of the Born contribution in Eq. 31 includes some one-loop effects in the first term which must be subtracted in order not to double count. This generates additional counterterms,

$$
\begin{aligned}
\frac{\delta \tilde{m}_b^h}{m_b} &= \Delta m_b \left(1 + \frac{1}{\tan\alpha \tan\beta} \right) \qquad (h \text{ production}) \\
\frac{\delta \tilde{m}_b^H}{m_b} &= \Delta m_b \left(1 - \frac{\tan\alpha}{\tan\beta} \right) \qquad (H \text{ production}) \\
\frac{\delta \tilde{m}_b^A}{m_b} &= \Delta m_b \left(1 + \frac{1}{\tan^2\beta} \right) \qquad (A \text{ production}).
\end{aligned}
\tag{40}
$$

The counterterms make a contribution to the total partonic SQCD cross section,

$$
\frac{d\hat{\sigma}_{CT}}{dt} = \frac{d\hat{\sigma}_{IBA}}{dt} \left(2\delta Z_V^b + \delta Z_3 + 2\delta Z_g + 2\frac{\delta m_b}{m_b} + 2\frac{\delta \tilde{m}_b^\phi}{m_b} \right).
\tag{41}
$$

We note that the $1/\epsilon$ contributions cancel in Eq. 41, although there are remaining finite pieces.

---

[5] The validity of this relation for the squark/gluino contributions to the SQCD renormalization is demonstrated in Ref. [33] and references therein.

F. Complete NLO Result

The complete $\mathcal{O}(\alpha_s^2)$ NLO prediction includes both the pure QCD NLO corrections and the squark/gluino NLO SQCD contributions, along with the Born contribution[6] ,

$$\sigma_{NLO}(pp \rightarrow b\phi)_{QCD+SQD} \equiv \sigma_{NLO}(pp \rightarrow b\phi)_{SQCD} + +\delta\sigma_{QCD} \, . \tag{42}$$

The curves labelled "Complete NLO" in Section IV correspond to Eq. 42 and represent the most accurate predictions available for the $pp \rightarrow b\phi$ MSSM cross sections.

IV. RESULTS AND DISCUSSION

Our NLO numerical results are obtained with CTEQ6M parton distributions[37], $\alpha_s(\mu_R)$ evaluated with the $2-$loop evolution and $\alpha_s^{NLO}(M_Z) = 0.118$, and use the Yukawa couplings of Eq. 17. The lowest order cross sections use CTEQ6L PDFs, $\alpha_s(\mu_R)$ evaluated at 1-loop, and have the lowest order Yukawa couplings of Eq. 8. We require that the outgoing b quark has $p_T > 20$ GeV and pseudorapidity $\mid \eta \mid < 2.0$ for the Tevatron and $\mid \eta \mid < 2.5$ for the LHC. In the NLO QCD real gluon emission contribution (obtained from Ref. [6]), the final state gluons and b quarks are merged into a single jet if their pseudorapidity/azimuthal separation, $\Delta R = \sqrt{(\Delta\eta)^2 + (\Delta\phi)^2}$, is less than 0.4. The renormalization/factorization scales, μ_R, μ_F, are taken to be $M_\phi/4$. Finally, the results labelled "Improved Born Approximation" (Eq. 29), use NLO PDFS and $\alpha_s(\mu_R)$ evaluated with the $2-$loop evolution and $\alpha_s^{NLO}(M_Z) = 0.118$.

The b quark mass appearing in the Yukawa couplings of Eqs. 8 and 17 is taken to be the running $\overline{MS}$ b quark mass and is evaluated at two loops for the NLO predictions and the IBA predictions and at $1-$loop for the LO predictions,

$$\overline{m}_b(\mu_R)_{1l} = m_b^{\text{pole}} \left[\frac{\alpha_s(\mu_R)}{\alpha_s(m_b^{\text{pole}})} \right]^{c_0/b_0} \, ,$$

$$\overline{m}_b(\mu_R)_{2l} = m_b^{\text{pole}} \left[\frac{\alpha_s(\mu_R)}{\alpha_s(m_b^{\text{pole}})} \right]^{c_0/b_0} \left[1 + \frac{c_0}{b_0} \left(c_1 - b_1 \right) \frac{\alpha_s(\mu_R) - \alpha_s(m_b^{\text{pole}})}{\pi} \right] \, , \tag{43}$$

---

[6] Note the the Born contribution is (arbitrarily for this purpose) assigned to $\sigma_{NLO}(pp \rightarrow b\phi)_{SQCD}$

TABLE I: b squark masses and mixing angles from [30]. All soft-SUSY breaking masses are taken equal to $M_{SUSY} = m_{\tilde{g}} = A_b = A_t$ and $\mu = M_2 = 200$ GeV.

M_{SUSY}(TeV)	$\tilde{\theta}_b$	$m_{\tilde{b}_1}$ (TeV)	$m_{\tilde{b}_2}$ (TeV)
		$\tan\beta = 10$	
1	-0.64	1.0	1.0
2	0.00	2.0	2.0
3	0.64	3.0	3.0
4	0.71	4.0	4.0
5	0.74	5.0	5.0

TABLE II: b squark masses and mixing angles from [30]. All soft-SUSY breaking masses are taken equal to $M_{SUSY} = m_{\tilde{g}} = A_b = A_t$ and $\mu = M_2 = 200$ GeV.

M_{SUSY}(TeV)	$\tilde{\theta}_b$	$m_{\tilde{b}_1}$ (TeV)	$m_{\tilde{b}_2}$ (TeV)
		$\tan\beta = 40$	
1	-0.76	1.0	.98
2	-0.76	2.0	2.0
3	-0.75	3.0	3.0
4	-0.75	4.0	4.0
5	-0.73	5.0	5.0

where,

$$b_0 = \frac{1}{4\pi}\left(\frac{11}{3}N_c - \frac{2}{3}N_{fl}\right), \qquad b_1 = \frac{1}{2\pi}\left(\frac{51N_c - 19N_{fl}}{11N_c - 2N_{fl}}\right),$$

$$c_0 = \frac{1}{\pi}, \qquad\qquad\qquad c_1 = \frac{1}{72\pi}\left(101N_c - 10N_{fl}\right) ,$$

with $N_c = 3$ and $N_{fl} = 5$, the number of light flavors. We take the b quark pole mass, $m_b^{\text{pole}} = 4.62$ GeV.

The MSSM parameters are found using FeynHiggs to generate an effective Higgs mixing angle, α_{eff}, and radiatively corrected Higgs masses. The MSSM parameters are listed in the figure captions. The gluino mass is always identified with M_{SUSY}, while the b squark masses and the b squark mixing angle, $\tilde{\theta}_b$, are given for representative parameter values in Tables I and II.
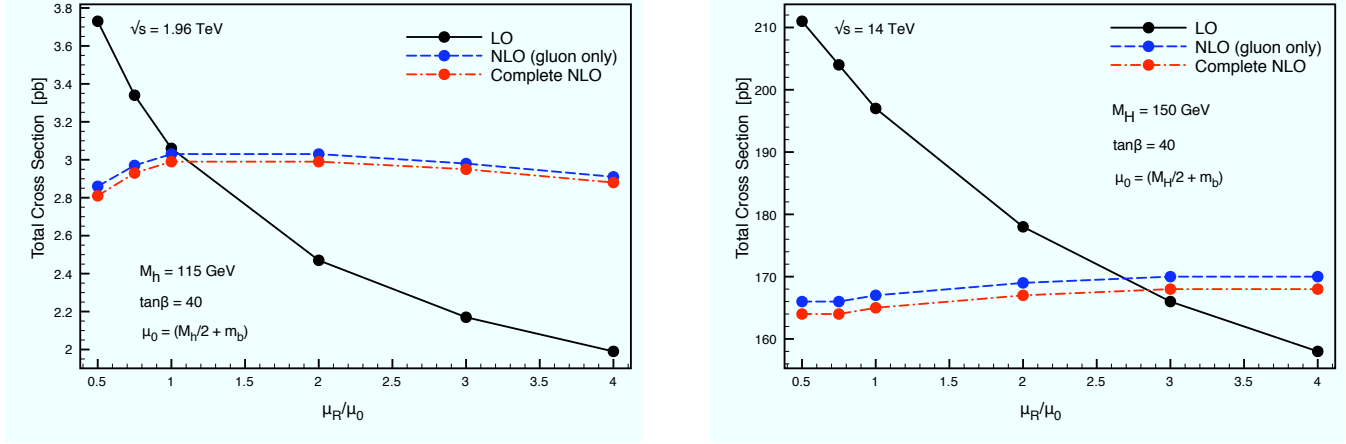
FIG. 4: Scale dependence of the NLO results for $p\overline{p} \to bh^0$ (LHS) and $pp \to bH^0$ (RHS) for $\tan\beta = 40$. We set the renormalization/factorization scales equal, $\mu_R = \mu_F$.

The NLO results for the $pp(p\overline{p}) \to b\phi$ processes depend on both the renormalization and factorization scales. For simplicity, we take these scales equal, $\mu_R = \mu_F$. Fig. 4 shows the dependence on scale (μ_R/μ_0) of the NLO results at both the Tevatron and the LHC and demonstrates the expected improvements between the lowest order results and the NLO results. The curves labelled "Complete NLO" include the full set of QCD and SQCD contributions (Eq. 42) and are significantly less dependent on the choice of scale than the lowest order result (Eq. 27). The dashed curve ("NLO (gluon only)", Eq. 28) only includes the SQCD contributions via the effective Yukawa couplings of Eq. 17 and has an almost identical scale dependence as the full result of Eq. 42. For the remainder of our plots, we choose the renormalization/factorization scale to be $M_\phi/4$.

Results for the lightest MSSM scalar, h^0, are shown in Figs. 5 and 6 for the Tevatron.[7] Fig. 5 shows the dependence of the complete set of SQCD contributions (Eq. 32) and the

---

[7] A preliminary study of the SQCD contributions to bh^0 production in the MSSM appears in Ref. [38]. This work used a renormalization framework in which the heavy squarks and gluino do not decouple and hence their results are not directly comparable to ours. We find, however, qualitative agreement with their results.

16

pure NLO QCD result (Eq. 28) on the lightest Higgs mass for $\tan\beta = 10$ and 40. The curve marked "gluon (only)" (Eq. 28) includes the NLO QCD corrections and uses the effective Yukawa couplings of Eq. 17, while the SQCD curve (Eq. 32) incorporates the full set of SQCD corrections (box diagrams, etc). We see that the effects of squark and gluino loops which are not absorbed into the the effective Yukawa couplings are typically less than $1-2\%$ for both $\tan\beta = 10$ and $\tan\beta = 40$ and can safely be neglected. We also note that the sizes of the NLO corrections (both pure QCD and SQCD) do not have strong dependences on the mass of the produced Higgs boson.

Fig. 6 compares the SQCD result (Eq. 32) with that obtained in the Improved Born Approximation (IBA), Eq. 29. For both values of $\tan\beta$ plotted, the Improved Born Approximation is an excellent approximation. This is an important result of our calculation because it demonstrates that the effective Lagrangian approach is extremely accurate for $b\phi$ production. It is apparent that the squark and gluino contributions which are not included in the IBA approximation give a negligible contribution to the rate. Figure 6 also exhibits the slow approach to the decoupling limit already noted in Ref. [25]. The decoupling limit, where the SQCD corrections do not contribute to the rate, corresponds to $\sigma_{NLO}/\sigma_{LO} - 1 = 0$ in this plot. The approach to the decoupling limit is significantly slower for large $\tan\beta$ than for small $\tan\beta$, as is apparent in Eq. 20. Even for M_{SUSY} as large as 5 TeV, the SQCD effects present in the couplings of the effective Lagrangian of Eq. 17 are still $\mathcal{O}(5\%)$ for $\tan\beta = 40$.

Results for the heavier neutral MSSM scalar, H^0, are shown in Figs. 7 and 8 for the LHC. Fig. 7 shows the dependence of the SQCD corrections on the heavy Higgs mass for $\tan\beta = 10$ and 40. The NLO pure QCD results (Eq. 28) are quite sensitive to M_H, while the SQCD corrections (Eq. 32) are relatively independent of the Higgs mass and quite small. The complete NLO rate including all QCD and SQCD effects (Eq. 42) differs by less than 1 % from the "NLO (gluon only)") calculation where the SQCD effects are included only via the Yukawa couplings of the effective Lagrangian. Fig. 8 compares the full SQCD result with that obtained in the Improved Born Approximation (IBA) and as is the case for the lighter Higgs boson, the Improved Born Approximation closely approximates the full SQCD calculation. The slow approach to the decoupling limit for the H^0 is similar to that seen for the h^0.

Results for the MSSM pseudoscalar, A^0, are shown in Figs. 9 and 10 for the LHC. Fig.
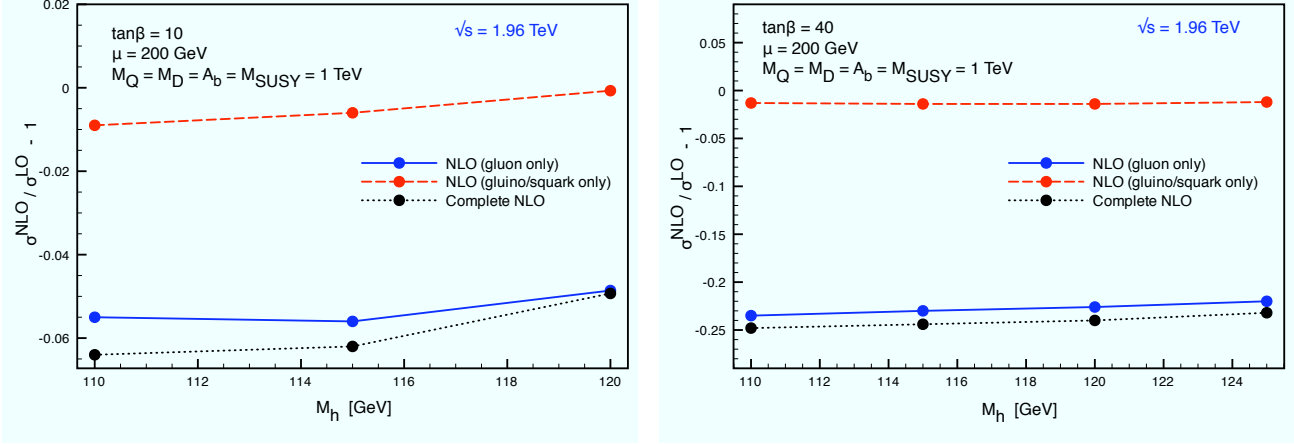
FIG. 5: Effects of NLO QCD and SQCD contributions on the rate for $pp \to bh^0$ at the LHC. The outgoing b quark satisfies $p_T > 20~GeV$ and $\mid \eta \mid < 2$. The NLO results use NLO PDFs, $2-$loop evolution of $\alpha_s(\mu_R)$ and $\overline{m_b}(\mu_R)$, and the Yukawa couplings of Eq. 17. The plots are normalized to the lowest order cross section of Eq. 26, which is computed with lowest order PDFs, 1-loop evolution of $\alpha_s(\mu_R)$ and $\overline{m_b}(\mu_R)$, and the lowest order Yukawa couplings, $g_{b\bar{b}h}^{LO}$.

9 shows the dependence of the SQCD corrections on the pseudoscalar mass for $\tan\beta = 10$ and 40. The SQCD effects (Eq. 32) are positive and are of a similar magnitude as those found for H^0 production and again are relatively independent of the Higgs mass, M_A. Fig. 10 compares the full SQCD result with that obtained in the Improved Born Approximation. In this case, the Improved Born Approximation gives a prediction which differs from the full SQCD rate by about -3% for both $\tan\beta = 10$ and 40 and we again see the slow approach to the decoupling limit. This plot fixes $M_A = 500~GeV$ and varies M_{SUSY}. From Eq. 21, it is clear that for decoupling to occur we need to also take $M_A \to \infty$. For fixed M_A, even for $M_{SUSY} = 5~TeV$, the effect of squark and gluino loops are still $\mathcal{O}(5-10)\%$.
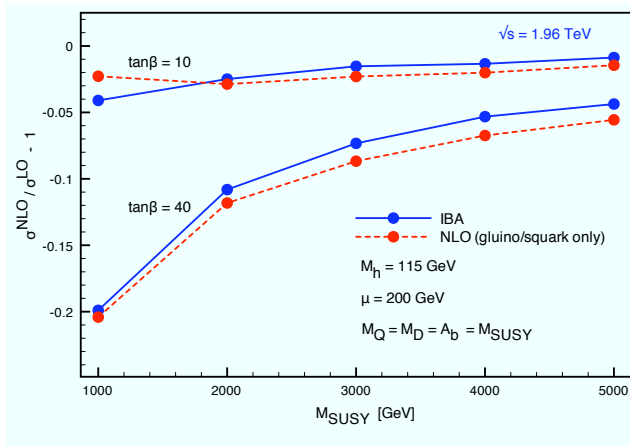
FIG. 6: Comparison of the full SQCD calculation (Eq. 32) with the Improved Born Approximation (Eq. 29) on the rate for $p\overline{p} \rightarrow bh^0$ at the Tevatron. The outgoing b quark satisfies $p_T > 20\ GeV$ and $| \eta |< 2$.

V.   CONCLUSIONS

We have computed the $\mathcal{O}(\alpha_s^2)$ SUSY QCD corrections from squark and gluino loops for the associated production of an MSSM Higgs boson and a b quark. When the Yukawa couplings are normalized with the effective Lagrangian of Eq. 17, the remaining SQCD corrections from squark and gluino loops are typically of order a few percent. We have therefore explicitly demonstrated that the effective Lagrangian approach to calculating the effects of squark and gluino loops is extremely accurate and can be reliably used to approximate the $b\phi$ cross sections. In Figs. 11 and 12, we summarize our results by showing the complete NLO predictions for b Higgs associated production at the Tevatron and the LHC.[8] These figures include all NLO $\mathcal{O}(\alpha_s^2)$ contributions and represent the most complete calculation available.

---

[8] The bh cross section decreases rapidly as the maximum allowed value of M_h is approached from below due to the suppression of the $b\overline{b}h$ coupling. Similarly, the bH cross section decreases as $M_{h,Max}$ is approached from above due to the suppression in this region of the $b\overline{b}H$ coupling.
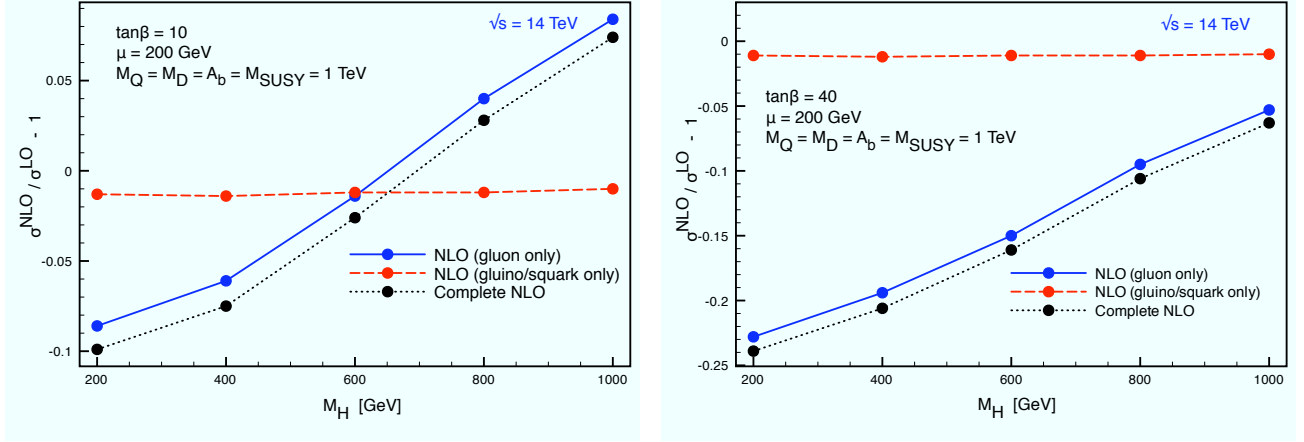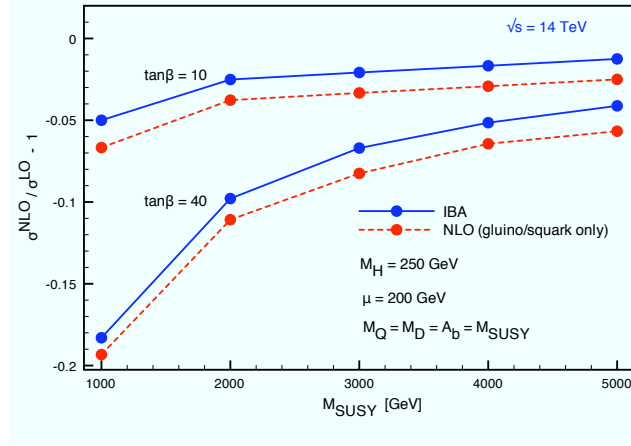
19

FIG. 7: Effects of NLO QCD and SQCD contributions on the rate for $pp \to bH^0$ at the LHC. The outgoing b quark satisfies $p_T > 20 \ GeV$ and $\mid \eta \mid < 2.5$. The NLO results use NLO PDFs, $2-$loop evolution of $\alpha_s(\mu_R)$ and $\overline{m_b}(\mu_R)$, and the Yukawa couplings of Eq. 17. The plots are normalized to the lowest order cross section of Eq. 26, which is computed with lowest order PDFs, 1-loop evolution of $\alpha_s(\mu_R)$ and $\overline{m_b}(\mu_R)$, and the lowest order Yukawa couplings, $g_{b\bar{b}h}^{LO}$.

Acknowledgments

FIG. 8: Comparison of the full SQCD calculation (Eq. 32) with the Improved Born Approximation (Eq. 29) for the rate for $pp \to bH^0$ at the LHC. The outgoing b quark satisfies $p_T > 20 \; GeV$ and $| \eta | < 2.5$.

APPENDIX A: SCALAR INTEGRALS AND TENSOR COEFFICIENTS

The scalar integrals are defined as:

$$
\begin{aligned}
\frac{i}{16\pi^2} A_0(M_0) &= \int \frac{d^n k}{(2\pi)^n} \frac{1}{N_0} \,, \\
\frac{i}{16\pi^2} B_0(p_1^2; M_0, M_1) &= \int \frac{d^n k}{(2\pi)^n} \frac{1}{N_0 N_1} \,, \\
\frac{i}{16\pi^2} C_0(p_1^2, p_2^2; M_0, M_1, M_2) &= \int \frac{d^n k}{(2\pi)^n} \frac{1}{N_0 N_1 N_2} \,, \\
\frac{i}{16\pi^2} D_0(p_1^2, p_2^2, p_3^2; M_0, M_1, M_2, M_3) &= \int \frac{d^n k}{(2\pi)^n} \frac{1}{N_0 N_1 N_2 N_3} \,,
\end{aligned}
\tag{A1}
$$

where:

$$
\begin{aligned}
N_0 &= k^2 - M_0^2 \\
N_1 &= (k + p_1)^2 - M_1^2 \\
N_2 &= (k + p_1 + p_2)^2 - M_2^2 \\
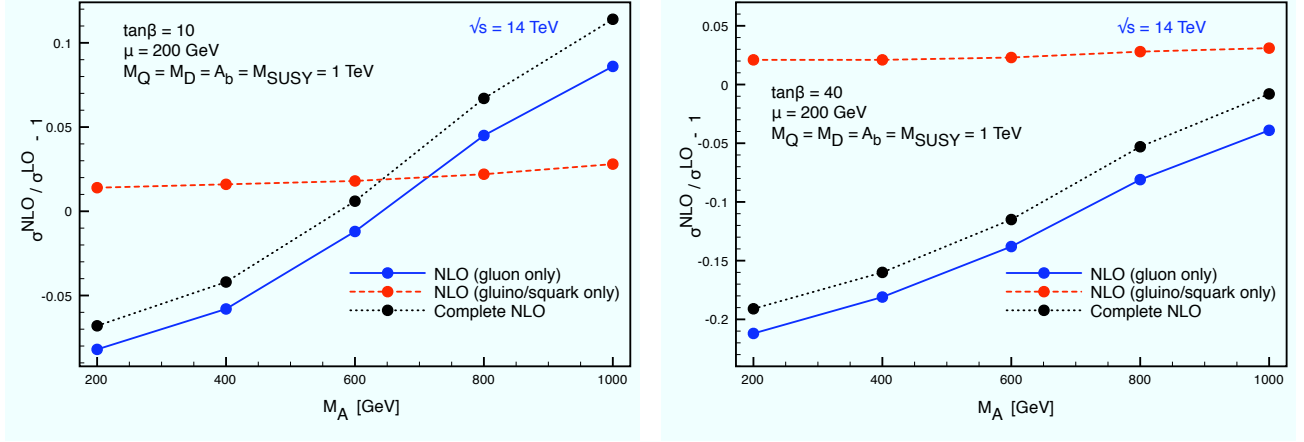N_3 &= (k + p_1 + p_2 + p_3)^2 - M_3^2 \,.
\end{aligned}
\tag{A2}
$$

21

FIG. 9: Effects of NLO QCD and SQCD contributions on the rate for $pp \to bA^0$ at the LHC. The outgoing b quark satisfies $p_T > 20 \ GeV$ and $| \ \eta \ |< 2.5$. The NLO results use NLO PDFs, $2-$loop evolution of $\alpha_s(\mu_R)$ and $\overline{m_b}(\mu_R)$, and the Yukawa couplings of Eq. 17. The plots are normalized to the lowest order cross section of Eq. 26, which is computed with lowest order PDFs, 1-loop evolution of $\alpha_s(\mu_R)$ and $\overline{m_b}(\mu_R)$, and the lowest order Yukawa couplings, g_{bbh}^{LO}.

The tensor integrals encountered are expanded in terms of the external momenta p_i and the metric tensor $g^{\mu\nu}$. For the two-point function we write:

$$
\begin{aligned}
\frac{i}{16\pi^2} B^\mu(p_1^2; M_0, M_1) &= \int \frac{d^n k}{(2\pi)^n} \frac{k^\mu}{N_0 N_1} \\
&\equiv \frac{i}{16\pi^2} p_1^\mu B_1(p_1^2, M_0, M_1),
\end{aligned} \tag{A3}
$$

while for the three-point functions we have both rank-one and rank-two tensor integrals which we expand as:

$$
\begin{aligned}
C^\mu(p_1^2, p_2^2; M_0, M_1, M_2) &= p_1^\mu C_{11} + p_2^\mu C_{12}, \\
C^{\mu\nu}(p_1^2, p_2^2; M_0, M_1, M_2) &= p_1^\mu p_1^\nu C_{21} + p_2^\mu p_2^\nu C_{22} \\
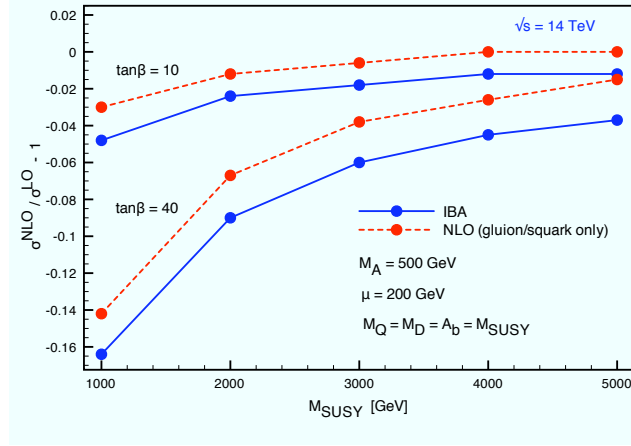&\quad + (p_1^\mu p_2^\nu + p_1^\nu p_2^\mu) C_{23} + g^{\mu\nu} C_{24},
\end{aligned} \tag{A4}
$$

FIG. 10: Comparison of the full SQCD calculation (Eq. 32) with the Improved Born Approximation (Eq. 29) for $pp \to bA^0$ at the LHC. The outgoing b quark satisfies $p_T > 20\ GeV$ and $\mid \eta \mid < 2.5$.
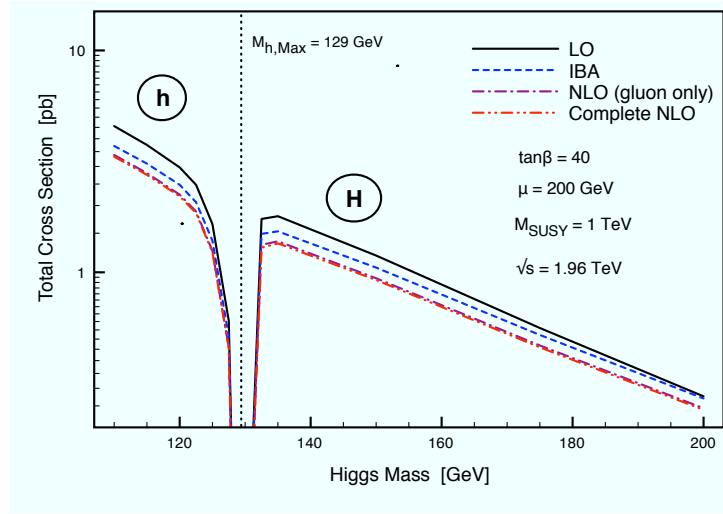

FIG. 11: Complete NLO $\mathcal{O}(\alpha_s^2)$ results for $p\bar{p} \to bh^0(H^0)$ at the Tevatron.

where:

$$\frac{i}{16\pi^2} C^\mu(C^{\mu\nu})(p_1^2, p_2^2; M_0, M_1, M_2) \equiv \int \frac{d^n k}{(2\pi)^n} \frac{k^\mu(k^\mu k^\nu)}{N_0 N_1 N_2} \qquad (A5)$$

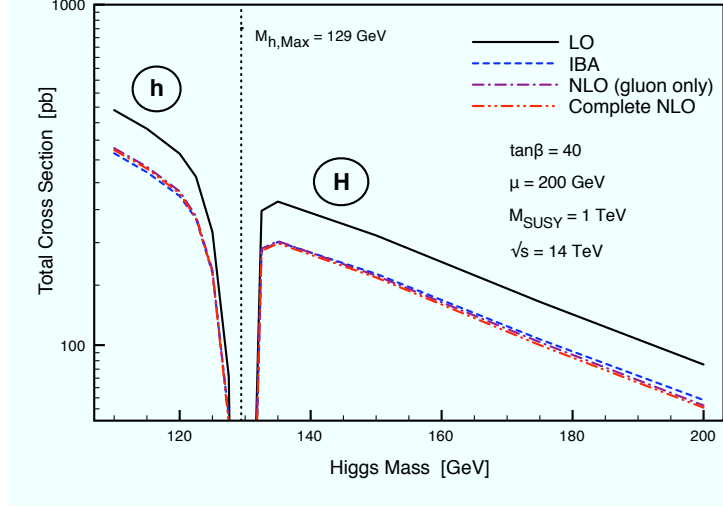Finally, for the box diagrams, we encounter only rank-one tensor integrals which are

23

FIG. 12: Complete NLO $\mathcal{O}(\alpha_s^2)$ results for $pp \to bh^0(H^0)$ at the LHC.

written in terms of the Passarino-Veltmann coefficients as:

$$
\begin{aligned}
\frac{i}{16\pi^2} D^\mu(p_1^2, p_2^2; M_0, M_1, M_2) &\equiv \int \frac{d^n k}{(2\pi)^n} \frac{k^\mu}{N_0 N_1 N_2 N_3} \\
&= \frac{i}{16\pi^2} \left\{ p_1^\mu D_{11} + p_2^\mu D_{12} + p_3^\mu D_{13} \right\}.
\end{aligned} \tag{A6}
$$

APPENDIX B: ONE LOOP SQCD COEFFICIENTS

The cofficients for each diagram are given below in the notation of Eq. 30. The self-energy contributions are shown in Fig. 13.
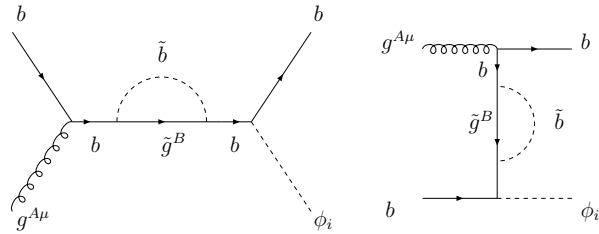

FIG. 13: Self- energy diagrams, S_1 and S_2.

Diagram S_1:

24

$$X_{S_1}^{(s)} = X_{S_1}^{(1)} = 0$$

$$X_{S_1}^{(t)} = -\frac{4}{3}g_{b\bar{b}\phi}\left[\frac{B_1(t; m_{\tilde{g}}, m_{\tilde{b}_1}) + B_1(t; m_{\tilde{g}}, m_{\tilde{b}_2})}{t}\right]. \tag{B1}$$

Diagram S_2:

$$X_{S_2}^{(s)} = -\frac{4}{3}g_{b\bar{b}\phi}\left[\frac{B_1(s; m_{\tilde{g}}, m_{\tilde{b}_1}) + B_1(s; m_{\tilde{g}}, m_{\tilde{b}_2})}{s}\right]$$

$$X_{S_2}^{(t)} = X_{S_2}^{(1)} = 0. \tag{B2}$$

The virtual diagrams are shown in Figs. 14, 15 and 16. An effective $b\bar{b}g$ vertex can be extracted from Figs. 14 and 15 and in the limit where the b quarks of the effective vertex are on-shell, our results agree with Ref. [33]. An effective $b\bar{b}\phi_i$ vertex can be found from Figs. 16 and agrees with the results of Refs. [22, 23, 25] when the b quarks are on shell.
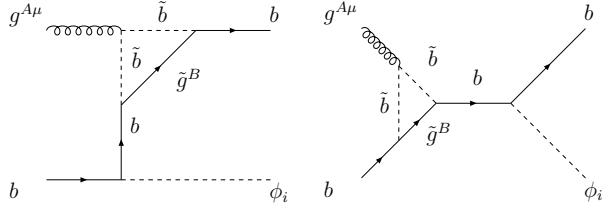

FIG. 14: Vertex diagrams, V_1 and V_2.

Diagram V_1 :

$$X_{V_1}^{(s)} = -\frac{g_{b\bar{b}\phi}}{6}\sum_{i=1}^{2}\left[C_{12} + C_{23}\right](0, 0; m_{\tilde{g}}, m_{\tilde{b}_i}, m_{\tilde{b}_i})$$

$$X_{V_1}^{(t)} = \frac{g_{b\bar{b}\phi}}{6}\sum_{i=1}^{2}\left[\frac{2}{t}C_{24} + C_{12} + C_{23}\right](0, 0; m_{\tilde{g}}, m_{\tilde{b}_i}, m_{\tilde{b}_i})$$

$$X_{V_1}^{(1)} = \frac{g_{b\bar{b}\phi}}{3}\sum_{i=1}^{2}\left[C_{12} + C_{23}\right](0, 0; m_{\tilde{g}}, m_{\tilde{b}_i}, m_{\tilde{b}_i}). \tag{B3}$$

Diagram V_2 :

$$X_{V_2}^{(s)} = \frac{g_{b\bar{b}\phi}}{3} \sum_{i=1}^{2} \frac{C_{24}}{s}(s, 0; m_{\tilde{g}}, m_{\tilde{b}_i}, m_{\tilde{b}_i})$$

$$X_{V_2}^{(t)} = 0$$

$$X_{V_2}^{(1)} = \frac{g_{b\bar{b}\phi}}{3} \sum_{i=1}^{2} \left[C_{11} - C_{12} + C_{21} - C_{23} \right] (s, 0; m_{\tilde{g}}, m_{\tilde{b}_i}, m_{\tilde{b}_i}) . \tag{B4}$$

FIG. 15: Vertex diagrams, V_3 and V_4.

$$X_{V_2}^{(s)} = \frac{g_{b\bar{b}\phi}}{3} \sum_{i=1}^{2} \frac{C_{24}}{s}(s, 0; m_{\tilde{g}}, m_{\tilde{b}_i}, m_{\tilde{b}_i})$$

$$X_{V_2}^{(t)} = 0$$

$$X_{V_2}^{(1)} = \frac{g_{b\bar{b}\phi}}{3} \sum_{i=1}^{2} \left[C_{11} - C_{12} + C_{21} - C_{23} \right] (s, 0; m_{\tilde{g}}, m_{\tilde{b}_i}, m_{\tilde{b}_i}) . \tag{B4}$$
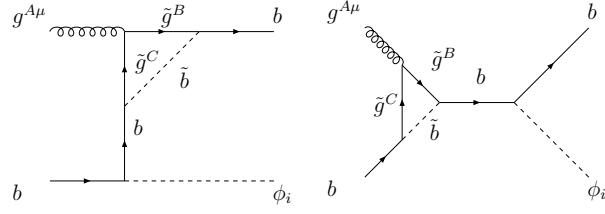

FIG. 15: Vertex diagrams, V_3 and V_4.

Diagram V_3 :

$$X_{V_3}^{(s)} = -\frac{3}{2}g_{b\bar{b}\phi}\sum_{i=1}^{2}\left[C_{12}+C_{23}\right](0,0;m_{\tilde{b}_i},m_{\tilde{g}},m_{\tilde{g}})$$

$$X_{V_3}^{(t)} = \frac{3}{2}g_{b\bar{b}\phi}\sum_{i=1}^{2}\left\{\left[\frac{1}{t}\left(2C_{24}+(m_{\tilde{g}}^2-m_{\tilde{b}_i}^2)C_0\right)+C_{23}\right](0,0;m_{\tilde{b}_i},m_{\tilde{g}},m_{\tilde{g}})\right.$$
$$\left.-\frac{B_0(0;m_{\tilde{g}},m_{\tilde{g}})}{t}\right\}$$

$$X_{V_3}^{(1)} = 3g_{b\bar{b}\phi}\sum_{i=1}^{2}\left[C_{12}+C_{23}\right](0,0;m_{\tilde{b}_i},m_{\tilde{g}},m_{\tilde{g}}). \tag{B5}$$
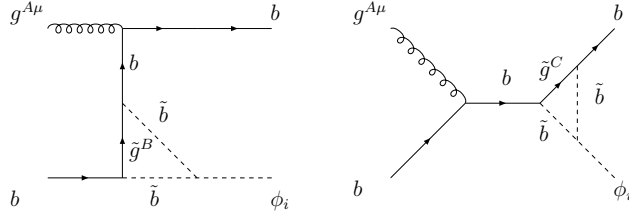

FIG. 16: Vertex diagrams, V_5 and V_6.

Diagram V_4 :

$$X_{V_4}^{(s)} = \frac{3}{2}g_{b\bar{b}\phi}\sum_{i=1}^{2}\left\{\left[\frac{1}{s}\left(2C_{24}+(m_{\tilde{g}}^2-m_{\tilde{b}_i}^2)C_0\right)-2C_{11}+C_{12}\right](s,0;m_{\tilde{b}_i},m_{\tilde{g}},m_{\tilde{g}})\right.$$
$$\left.-\frac{B_0(0;m_{\tilde{g}},m_{\tilde{g}})}{s}\right\}$$

$$X_{V_4}^{(t)} = 0$$

$$X_{V_4}^{(1)} = 3g_{b\bar{b}\phi}\sum_{i=1}^{2}\left[C_{11}-C_{12}+C_{21}-C_{23}\right](s,0;m_{\tilde{b}_i},m_{\tilde{g}},m_{\tilde{g}}). \tag{B6}$$

Diagram V_5 :

$$X_{V_5}^{(s)} = X_{V_5}^{(1)} = 0$$

$$X_{V_5}^{(t)} = \frac{4}{3}\left(\frac{m_{\tilde{g}}}{t}\right)\left\{2\cos\tilde{\theta}_b\sin\tilde{\theta}_b\left[\tilde{C}_{i22}C_0(m_{\tilde{b}_2}^2,m_{\tilde{b}_2}^2)-\tilde{C}_{i11}C_0(m_{\tilde{b}_1}^2,m_{\tilde{b}_1}^2)\right]\right.$$
$$\left.+(\cos^2\tilde{\theta}_b-\sin^2\tilde{\theta}_b)\tilde{C}_{i12}\left[C_0(m_{\tilde{b}_1}^2,m_{\tilde{b}_2}^2)+C_0(m_{\tilde{b}_2}^2,m_{\tilde{b}_1}^2)\right]\right\}, \tag{B7}$$

27

where the full arguments of the scalar integral and tensor coefficients are $(p_1^2, p_2^2; m_1^2, m_2^2, m_3^2) = (0, t; m_{\tilde{b}_i}^2, m_{\tilde{g}}^2, m_{\tilde{b}_j}^2)$.

Diagram V_6 :

$$
\begin{aligned}
X_{V_6}^{(s)} &= \frac{4}{3}\left(\frac{m_{\tilde{g}}}{s}\right)\left\{2\cos\tilde{\theta}_b\sin\tilde{\theta}_b\left[\tilde{C}_{i22}C_0(m_{\tilde{b}_2}^2, m_{\tilde{b}_2}^2) - \tilde{C}_{i11}C_0(m_{\tilde{b}_1}^2, m_{\tilde{b}_1}^2)\right]\right. \\
&\quad \left. +(\cos^2\tilde{\theta}_b - \sin^2\tilde{\theta}_b)\tilde{C}_{i12}\left[C_0(m_{\tilde{b}_1}^2, m_{\tilde{b}_2}^2) + C_0(m_{\tilde{b}_2}^2, m_{\tilde{b}_1}^2)\right]\right\} \\
X_{V_6}^{(t)} &= X_{V_6}^{(1)} = 0\,,
\end{aligned}
\tag{B8}
$$

where the full arguments of the scalar integral and tensor coefficients are $(p_1^2, p_2^2; m_1^2, m_2^2, m_3^2) = (0, s; m_{\tilde{b}_i}^2, m_{\tilde{g}}^2, m_{\tilde{b}_j}^2)$.
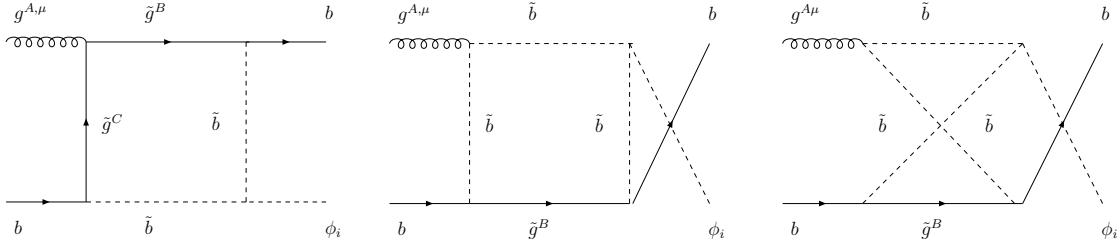
1. The Box Diagrams

FIG. 17: Box diagrams B_1, B_2 and B_3.

The box diagrams are shown in Fig. 17. The results of Eqs. B9, B10 and B11 sum over the contributions of $\tilde{b}_1$ and $\tilde{b}_2$.

Diagram B_1:

$$X_{B_1}^{(s)} = \frac{3}{2}m_{\tilde{g}}\left\{\sin 2\tilde{\theta}_b\left[\tilde{C}_{i22}(D_0+D_{13})(m_{\tilde{b}_2}^2,m_{\tilde{b}_2}^2)-\tilde{C}_{i11}(D_0+D_{13})(m_{\tilde{b}_1}^2,m_{\tilde{b}_1}^2)\right]\right.$$
$$\left.+\cos 2\tilde{\theta}_b\tilde{C}_{i12}\left[(D_0+D_{13})(m_{\tilde{b}_1}^2,m_{\tilde{b}_2}^2)+(D_0+D_{13})(m_{\tilde{b}_2}^2,m_{\tilde{b}_1}^2)\right]\right\}$$

$$X_{B_1}^{(t)} = -\frac{3}{2}m_{\tilde{g}}\left\{\sin 2\tilde{\theta}_b\left[\tilde{C}_{i22}D_{13}(m_{\tilde{b}_2}^2,m_{\tilde{b}_2}^2)-\tilde{C}_{i11}D_{13}(m_{\tilde{b}_1}^2,m_{\tilde{b}_1}^2)\right]\right.$$
$$\left.+\cos 2\tilde{\theta}_b\tilde{C}_{i12}\left[D_{13}(m_{\tilde{b}_1}^2,m_{\tilde{b}_2}^2)+D_{13}(m_{\tilde{b}_2}^2,m_{\tilde{b}_1}^2)\right]\right\}$$

$$X_{B_1}^{(1)} = 3m_{\tilde{g}}\left\{\sin 2\tilde{\theta}_b\left[\tilde{C}_{i22}(D_{11}-D_{13})(m_{\tilde{b}_2}^2,m_{\tilde{b}_2}^2)-\tilde{C}_{i11}(D_{11}-D_{13})(m_{\tilde{b}_1}^2,m_{\tilde{b}_1}^2)\right]\right.$$
$$\left.+\cos 2\tilde{\theta}_b\tilde{C}_{i12}\left[(D_{11}-D_{13})(m_{\tilde{b}_1}^2,m_{\tilde{b}_2}^2)+(D_{11}-D_{13})(m_{\tilde{b}_2}^2,m_{\tilde{b}_1}^2)\right]\right\}, \qquad \text{(B9)}$$

where the full arguments of the scalar integral and tensor coefficients are $(p_1^2,p_2^2,p_3^2;m_1,m_2,m_3,m_4)=(0,0,0;m_{\tilde{b}_i},m_{\tilde{g}},m_{\tilde{g}}^2,m_{\tilde{b}_j}^2)$.

Diagram B_2:

$$X_{B_2}^{(s)} = \frac{1}{6}m_{\tilde{g}}\left\{\sin 2\tilde{\theta}_b\left[\tilde{C}_{i22}D_{13}(m_{\tilde{b}_2}^2,m_{\tilde{b}_2}^2)-\tilde{C}_{i11}D_{13}(m_{\tilde{b}_2}^2,m_{\tilde{b}_2}^2)\right]\right.$$
$$\left.+\cos 2\tilde{\theta}_b\tilde{C}_{i12}\left[D_{13}(m_{\tilde{b}_1}^2,m_{\tilde{b}_2}^2)+D_{13}(m_{\tilde{b}_2}^2,m_{\tilde{b}_1}^2)\right]\right\}$$

$$X_{B_2}^{(t)} = -\frac{1}{6}m_{\tilde{g}}\left\{\sin 2\tilde{\theta}_b\left[\tilde{C}_{i22}D_{13}(m_{\tilde{b}_2}^2,m_{\tilde{b}_2}^2)+\tilde{C}_{i11}D_{13}(m_{\tilde{b}_1}^2,m_{\tilde{b}_1}^2)\right]\right.$$
$$\left.+\cos 2\tilde{\theta}_b\tilde{C}_{i12}\left[D_{13}(m_{\tilde{b}_1}^2,m_{\tilde{b}_2}^2)+D_{13}(m_{\tilde{b}_2}^2,m_{\tilde{b}_1}^2)\right]\right\}$$

$$X_{B_2}^{(1)} = \frac{1}{3}m_{\tilde{g}}\left\{\sin 2\tilde{\theta}_b\left[\tilde{C}_{i22}(D_{12}-D_{13})(m_{\tilde{b}_2}^2,m_{\tilde{b}_2}^2)-\tilde{C}_{i11}(D_{12}-D_{13})(m_{\tilde{b}_1}^2,m_{\tilde{b}_1}^2)\right]\right.$$
$$\left.+\cos 2\tilde{\theta}_b\tilde{C}_{i12}\left[(D_{12}-D_{13})(m_{\tilde{b}_1}^2,m_{\tilde{b}_2}^2)+(D_{12}-D_{13})(m_{\tilde{b}_2}^2,m_{\tilde{b}_1}^2)\right]\right\}, \qquad \text{(B10)}$$

where the arguments of the scalar integral and tensor coefficients are $(p_1^2,p_2^2,p_3^2;m_1^2,m_2^2,m_3^2,m_4^2)=(0,0,0;m_{\tilde{b}_i},m_{\tilde{b}_i},m_{\tilde{g}},m_{\tilde{b}_j})$.

Diagram B_3:

$$X_{B_3}^{(s)} = -\frac{1}{6}m_{\tilde{g}}\left\{\sin 2\tilde{\theta}_b\left[\tilde{C}_{i22}D_{13}(m_{\tilde{b}_2}^2, m_{\tilde{b}_2}^2) - \tilde{C}_{i11}D_{13}(m_{\tilde{b}_2}^2, m_{\tilde{b}_2}^2)\right]\right.$$
$$\left. + \cos 2\tilde{\theta}_b\tilde{C}_{i12}\left[D_{13}(m_{\tilde{b}_1}^2, m_{\tilde{b}_2}^2) + D_{13}(m_{\tilde{b}_2}^2, m_{\tilde{b}_1}^2)\right]\right\}$$

$$X_{B_3}^{(t)} = \frac{1}{6}m_{\tilde{g}}\left\{\sin 2\tilde{\theta}_b\left[\tilde{C}_{i22}D_{13}(m_{\tilde{b}_2}^2, m_{\tilde{b}_2}^2) + \tilde{C}_{i11}D_{13}(m_{\tilde{b}_1}^2, m_{\tilde{b}_1}^2)\right]\right.$$
$$\left. + \cos 2\tilde{\theta}_b\tilde{C}_{i12}\left[D_{13}(m_{\tilde{b}_1}^2, m_{\tilde{b}_2}^2) + D_{13}(m_{\tilde{b}_2}^2, m_{\tilde{b}_1}^2)\right]\right\}$$

$$X_{B_3}^{(1)} = \frac{1}{3}m_{\tilde{g}}\left\{\sin 2\tilde{\theta}_b\left[\tilde{C}_{i22}(D_{12} - D_{13})(m_{\tilde{b}_2}^2, m_{\tilde{b}_2}^2) - \tilde{C}_{i11}(D_{12} - D_{13})(m_{\tilde{b}_1}^2, m_{\tilde{b}_1}^2)\right]\right.$$
$$\left. + \cos 2\tilde{\theta}_b\tilde{C}_{i12}\left[(D_{12} - D_{13})(m_{\tilde{b}_1}^2, m_{\tilde{b}_2}^2) + (D_{12} - D_{13})(m_{\tilde{b}_2}^2, m_{\tilde{b}_1}^2)\right]\right\}, \qquad \text{(B11)}$$

where the arguments of the scalar integral and tensor coefficients are $(p_1^2, p_2^2, p_3^2; m_1, m_2, m_3, m_4) = (0, 0, 0; m_{\tilde{b}_i}, m_{\tilde{b}_i}, m_{\tilde{g}}, m_{\tilde{b}_j})$.

---

[1] S. Dawson, C. B. Jackson, L. Reina, and D. Wackeroth. Higgs production in association with bottom quarks at hadron colliders. *Mod. Phys. Lett.*, A21:89–110, 2006.

[2] Marcela S. Carena, A. Menon, and C. E. M. Wagner. Challenges for mssm higgs searches at hadron colliders. *Phys. Rev.*, D76:035004, 2007.

[3] J. Campbell et al. Higgs boson production in association with bottom quarks. 2004.

[4] Stefan Dittmaier, Michael Kramer, and Michael Spira. Higgs radiation off bottom quarks at the tevatron and the lhc. *Phys. Rev.*, D70:074010, 2004.

[5] Marcela S. Carena, S. Mrenna, and C. E. M. Wagner. Mssm higgs boson phenomenology at the tevatron collider. *Phys. Rev.*, D60:075010, 1999.

[6] S. Dawson, C. B. Jackson, L. Reina, and D. Wackeroth. Higgs boson production with one bottom quark jet at hadron colliders. *Phys. Rev. Lett.*, 94:031802, 2005.

[7] S. Dawson, C. B. Jackson, L. Reina, and D. Wackeroth. Exclusive higgs boson production with bottom quarks at hadron colliders. *Phys. Rev.*, D69:074027, 2004.

[8] F. Maltoni, Z. Sullivan, and S. Willenbrock. Higgs-boson production via bottom-quark fusion. *Phys. Rev.*, D67:093005, 2003.

[9] Fabio Maltoni, Thomas McElmurry, and Scott Willenbrock. Inclusive production of a higgs or z boson in association with heavy quarks. *Phys. Rev.*, D72:074024, 2005.

[10] D. Dicus, T. Stelzer, Z. Sullivan, and S. Willenbrock. Higgs boson production in association with bottom quarks at next-to-leading order. *Phys. Rev.*, D59:094016, 1999.

[11] J. Campbell, R. Keith Ellis, F. Maltoni, and S. Willenbrock. Higgs boson production in association with a single bottom quark. *Phys. Rev.*, D67:095002, 2003.

[12] R. Michael Barnett, Howard E. Haber, and Davison E. Soper. Ultraheavy particle production from heavy partons at hadron colliders. *Nucl. Phys.*, B306:697, 1988.

[13] Fredrick I. Olness and Wu-Ki Tung. When is a heavy quark not a parton? charged higgs production and heavy quark mass effects in the qcd based parton model. *Nucl. Phys.*, B308:813, 1988.

[14] Robert V. Harlander and William B. Kilgore. Higgs boson production in bottom quark fusion at next-to- next-to-leading order. *Phys. Rev.*, D68:013001, 2003.

[15] Anton Anastassov. Searches for higgs bosons at the tevatron. *AIP Conf. Proc.*, 903:73–80, 2007.

[16] Stefan Dittmaier, Michael Kramer, Alexander Muck, and Tobias Schluter. Mssm higgs-boson production in bottom-quark fusion: Electroweak radiative corrections. *JHEP*, 03:114, 2007.

[17] Oliver Brein and Wolfgang Hollik. Mssm higgs bosons associated with high-p(t) jets at hadron colliders. *Phys. Rev.*, D68:095006, 2003.

[18] Oliver Brein and Wolfgang Hollik. Distributions for mssm higgs boson + jet production at hadron colliders. *Phys. Rev.*, D76:035002, 2007.

[19] Oliver Brein and Wolfgang Hollik. Distributions for higgs + jet at hadron colliders: Mssm vs sm. 2007.

[20] B. Field, S. Dawson, and J. Smith. Scalar and pseudoscalar higgs boson plus one jet production at the lhc and tevatron. *Phys. Rev.*, D69:074013, 2004.

[21] B. Field, L. Reina, and C. B. Jackson. Higgs boson production with one bottom quark including higher-order soft-gluon corrections. 2007.

[22] Marcela S. Carena, David Garcia, Ulrich Nierste, and Carlos E. M. Wagner. Effective lagrangian for the anti-t b h+ interaction in the mssm and charged higgs phenomenology. *Nucl. Phys.*, B577:88–120, 2000.

[23] Lawrence J. Hall, Riccardo Rattazzi, and Uri Sarid. The top quark mass in supersymmetric

so(10) unification. *Phys. Rev.*, D50:7048–7065, 1994.

[24] Marcela S. Carena, A. Menon, R. Noriega-Papaqui, A. Szynkman, and C. E. M. Wagner. Constraints on b and higgs physics in minimal low energy supersymmetric models. *Phys. Rev.*, D74:015009, 2006.

[25] Howard E. Haber et al. Susy-qcd corrections to the mssm h0 b anti-b vertex in the decoupling limit. *Phys. Rev.*, D63:055004, 2001.

[26] Jaume Guasch, Petra Hafliger, and Michael Spira. Mssm higgs decays to bottom quark pairs revisited. *Phys. Rev.*, D68:115001, 2003.

[27] John F. Gunion, Howard E. Haber, Gordon L. Kane, and Sally Dawson. *THE HIGGS HUNTER'S GUIDE.* Addison Wesley (Menlo Park), 1990.

[28] Abdelhak Djouadi. The anatomy of electro-weak symmetry breaking. ii: The higgs bosons in the minimal supersymmetric model. 2005.

[29] Marcela S. Carena and Howard E. Haber. Higgs boson theory and phenomenology. ((v)). *Prog. Part. Nucl. Phys.*, 50:63–152, 2003.

[30] Thomas Hahn, Wolfgang Hollik, Sven Heinemeyer, and Georg Weiglein. Precision higgs masses with feynhiggs 2.2. 2005.

[31] S. Heinemeyer, W. Hollik, and G. Weiglein. Electroweak precision observables in the minimal supersymmetric standard model. *Phys. Rept.*, 425:265–368, 2006.

[32] Ansgar Denner, H. Eck, O. Hahn, and J. Kublbeck. Feynman rules for fermion number violating interactions. *Nucl. Phys.*, B387:467–484, 1992.

[33] Stefan Berge, Wolfgang Hollik, Wolf M. Mosle, and Doreen Wackeroth. Susy qcd one-loop effects in (un)polarized top-pair production at hadron colliders. *Phys. Rev.*, D76:034016, 2007.

[34] Marcela S. Carena, M. Olechowski, S. Pokorski, and C. E. M. Wagner. Electroweak symmetry breaking and bottom - top yukawa unification. *Nucl. Phys.*, B426:269–300, 1994.

[35] Petra Hafliger and Michael Spira. Associated higgs boson production with heavy quarks in e+ e- collisions: Susy-qcd corrections. *Nucl. Phys.*, B719:35–52, 2005.

[36] P. Nason, S. Dawson, and R. Keith Ellis. The total cross-section for the production of heavy quarks in hadronic collisions. *Nucl. Phys.*, B303:607, 1988.

[37] H. L. Lai et al. Global QCD analysis of parton structure of the nucleon: Cteq5 parton distributions. *Eur. Phys. J.*, C12:375–392, 2000.

[38] Jun-jie Cao, Guang-ping Gao, Robert J. Oakes, and Jin Min Yang. Higgs-boson production

associated with a bottom quark at hadron colliders with supersymmetric qcd corrections. *Phys. Rev.*, D68:075012, 2003.